DOI: 10.1002/ange.201310412

Anode Materials

Scalable Synthesis of Interconnected Porous Silicon/Carbon Composites by the Rochow Reaction as High-Performance Anodes of Lithium Ion Batteries**

*Zailei Zhang, Yanhong Wang, Wenfeng Ren, Qiangqiang Tan, Yunfa Chen, Hong Li, Ziyi Zhong, and Fabing Su**

Abstract: *Despite the promising application of porous Si-based anodes in future Li ion batteries, the large-scale synthesis of these materials is still a great challenge. A scalable synthesis of porous Si materials is presented by the Rochow reaction, which is commonly used to produce organosilane monomers for synthesizing organosilane products in chemical industry. Commercial Si microparticles reacted with gas CH_3Cl over various Cu-based catalyst particles to substantially create macropores within the unreacted Si accompanying with carbon deposition to generate porous Si/C composites. Taking advantage of the interconnected porous structure and conductive carbon-coated layer after simple post treatment, these composites as anodes exhibit high reversible capacity and long cycle life. It is expected that by integrating the organosilane synthesis process and controlling reaction conditions, the manufacture of porous Si-based anodes on an industrial scale is highly possible.*

Nanostructured porous silicon (Si) materials have potential applications in a wide range of emerging technologies, such as nanoelectronics,[1a] photonics,[1b] biosensors,[1c] microsensors,[1d] transistors,[1e] solar cells,[1f] thermoelectric nanodevices,[1g] therapeutic and diagnostic agents,[1h] and Li ion batteries.[1i–l] More recently, remarkable attention has been paid to their application as anodes in next generation Li ion batteries with high energy density and power performance that can be used for potable electronics, electric vehicles, and renewable energy storage.[2a] This is primarily because of the large theoretical capacity (4200 mA h g^{-1} versus 372 mA h g^{-1} for commercial graphite anodes), abundant resource, and high safety of Si-based anodes.[2b] However, Si anodes inevitably experience two critical problems upon Li insertion and extraction during charge–discharge cycles: the large volume changes (around 300%), which often leads to the structure fracture, pulverization, and the damage of mechanical integrity of the electrode, and the much lower conductivity of Si compared with the carbon anodes.[2c] As a result, Si-based electrodes normally suffer a rapid capacity fading upon cycling and thus degradation of electrochemical performance.

Many pioneering works have shown that the Si nanostructures with predefined void space and/or a conductive buffer layer can substantially accommodate the Si volume change preventing the fracture formation and improving their conductivity.[3a] These nanostructures include Si nanowires,[3b] Si nanospheres,[3c] Si nanotubes,[3d] Si nanoparticles,[3e] porous Si,[3f] Si/C nanospheres,[3g] Si/C microwires grown on graphite microspheres,[3h] mixed Si nanopowder with alginate,[1j] Si nanoparticles embedded within carbon,[3i] Si-coated carbon,[3j] graphene-encapsulated Si,[3k] Ag-coated Si,[3l] conductive polymer-coated Si,[3m] and carbon-coated Si.[3n] All the above Si-based anode materials have brought significant improvement to the electrochemical properties (capacity, cycle life, and rate performance) and understanding to the fundamental issues.[1i] Meanwhile, the instructive guidelines for designing high-performance Si anodes have been established.[2b] The methods used to prepare Si-based anode materials include chemical reduction of silica materials using Mg powders,[4a,b] noble metal-assisted chemical etching,[3l] solvothermal method,[3c] chemical vapor deposition (CVD) with various Si precursors,[3f,j] and pyrolysis of butyl-capped Si gels.[3n] However, these methods often have some critical drawbacks, such as the harsh reaction conditions (high temperature), high cost (noble metals), toxic reactants (SiH_4), tedious processes, and particularly the small scale synthesis and low productivity, limiting their large-scale application. Among the developed Si-based materials, porous Si, and Si/C composites have been demonstrated as one of the most promising anodes.[1l] However, nowadays how to realize a large scale production of porous Si-based anodes is still a great challenge, even a number of low-cost raw materials[4a–c] and simple processes[3i,4d] have been tested.

Herein, we report a scalable synthesis of the interconnected porous Si/C composites by the Rochow reaction, which was discovered in 1940s[5a] and is still the most economical route to produce organosilane monomers in chemical industry. The global output of organosilane monomers is about millions tons per year, which means the

[*] Z. Zhang, Dr. Y. Wang, W. Ren, Prof. Q. Tan, Prof. Y. Chen, Prof. Dr. F. Su
State Key Laboratory of Multiphase Complex Systems
Institute of Process Engineering, Chinese Academy of Sciences
Beijing 100190 (China)
fbsu@ ipe.ac.cn
Prof. H. Li
Institute of Physics, Chinese Academy of Sciences
Beijing 100190 (China)
Dr. Z. Zhong
Institute of Chemical Engineering and Sciences, A*star
1 Pesek Road, Jurong Island, Singapore 627833 (Singapore)

[**] We gratefully acknowledge the supports from the National Natural Science Foundation of China (Nos. 51272252 and 21031005).

Supporting information for this article is available on the WWW under http://dx.doi.org/10.1002/anie.201310412.

 © 2014 Wiley-VCH Verlag GmbH & Co. KGaA, Weinheim

consumption of millions tons of metallurgical-grade Si. Previously, we demonstrated the use of waste contact mass (the mixture of residual or unreacted Si particles with deactivated Cu-based catalysts) generated from organosilane industry to decorate graphite anode to enhance electrochemical performance.[5b] Inspired by this work, now we rationally prepare porous Si/C anode materials by controlling the Rochow reaction conditions. After recovery of Cu compounds followed by facile post treatment, the obtained Si/C materials as anodes of Li-ion batteries show good electrochemical performance.

The material preparation process is shown in Scheme 1. The industrial metallurgical-grade Si powder and Cu-based

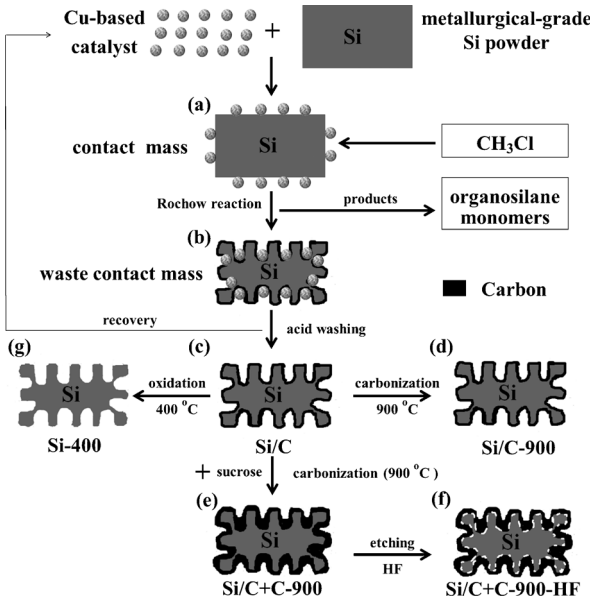

Scheme 1. The preparation process of porous Si/C materials.

catalyst particles are homogeneously ground to form a contact mass (Scheme 1a), which reacts with gas CH_3Cl to produce various organosilane monomers, and meanwhile, generates the waste contact mass (Scheme 1b). The latter is composed of unreacted Si, metal compounds, and deposited carbon. After removal or recovery of metal components by acid washing, the Si/C sample (Scheme 1c) is obtained. To increase the graphitic degree of materials, the Si/C sample is carbonized in N_2 at 900 °C to obtain the sample of Si/C-900 (Scheme 1d). To further increase the carbon content, Si/C is coated with sucrose and carbonized at 900 °C (Si/C + C-900 in Scheme 1e), followed by washing with HF solution to remove trace SiO_x and generate more interfacial space between the Si and the coated carbon layer.[6] The obtained sample is denoted Si/C + C-900-HF (Scheme 1f). The pure porous Si is obtained by calcination of Si/C in air at 400 °C to remove the carbon, and named Si-400 (Scheme 1g). The Rochow reaction conditions used for synthesizing all of the samples are compiled in the Supporting Information, Table S1.

Figure 1 shows the SEM images of metallurgical-grade bulk Si and the obtained porous Si/C. It can be seen that bulk Si microparticles in Figure 1a have a size range of about 10–

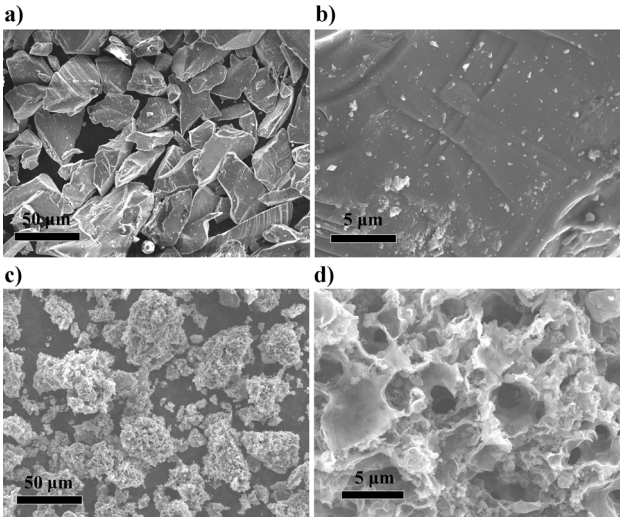

Figure 1. SEM images of reactant bulk Si powder (a, b) and porous Si/C (c, d).

100 μm before Rochow reaction, and their surface is smooth and dense (Figure 1b). After the catalytic reaction, porous Si/C particles with a size distribution of 2–60 μm (Figure 1c) are formed, which exhibit a coherent macroscopic porous network structure with a pore size of 1–5 μm (Figure 1d). The SEM images of other porous Si/C samples (Supporting Information, Figure S1) obtained under different reaction conditions also show that Si/C materials with internal connected porous structures can be readily prepared at a relatively low temperature of 325–450 °C using different Cu-based catalysts, such as Cu_2O,[7a] CuO,[7b] $Cu/Cu_2O/CuO$,[7c] and CuCl.[7d] After simple post treatments, Si/C-900 (Supporting Information, Figure S2a), Si/C + C-900 (Figure S2b), Si/C + C-900-HF (Figure S2c), and Si-400 (Figure S2d) also show porous structure. As we know, when the Cu-based catalyst and the Si powder are heated together at elevated temperatures in the presence of CH_3Cl, Cu_xSi as the catalytic active species is formed at the interface between the Cu-based catalyst and Si.[8a] Subsequently, by the reaction of Si with CH_3Cl, the gas products, mainly including CH_3SiCl_3, $(CH_3)_2SiCl_2$, $(CH_3)_3SiCl$, CH_3SiHCl_2, and $(CH_3)_2SiHCl$, are produced,[8b] which can be used as the organosilane monomers for production of organosilane materials in chemical industry. Meanwhile, bulk Si particles is etched or "drilled" to create numerous macropores on the Si surface. Upon prolonging the reaction time, these pores are connected each other. Furthermore, the large amount of deposited carbon is formed on the Si surface with prolonging the reaction time and/or raising the reaction temperature.[8c] Thus, macroporous Si/C materials can be obtained and their porous structure could be tailored by controlling proper reaction conditions and the Cu-based catalysts.

Figure 2a shows the XRD patterns of the waste contact mass, Si/C, Si/C-900, Si/C + C-900, Si/C + C-900-HF, and Si-400. The group peaks at about 28.3, 47.0, and 55.8° are assigned to (111), (220), and (311) diffractions of Si phase (JCPDS NO. 27-1402), while those at 43.3 and 50.5° to the (111) and (200) diffractions of Cu with cubic symmetry

© 2014 Wiley-VCH Verlag GmbH & Co. KGaA, Weinheim

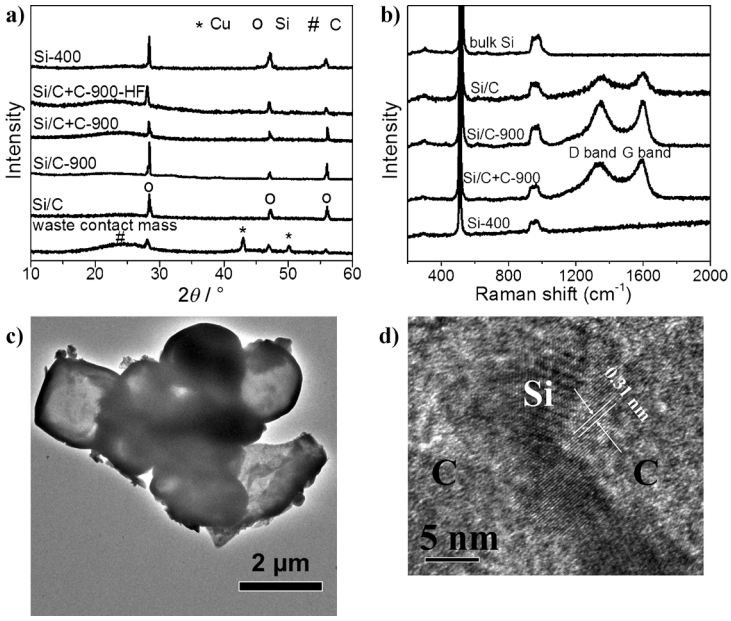

Figure 2. XRD patterns (a) and Raman spectra (b) of different samples, and TEM images of Si/C-900 (c, d).

(JCPDS No. 01-070-3039). After the acid washing, these Cu peaks disappeared. Besides the Si phase, the weak carbon peak at about 25.0° (002) is also observed for the waste contact mass, Si/C + C-900, and Si/C + C-900-HF. The carbon peak for Si/C + C-900 and Si/C + C-900-HF becomes stronger than that of Si/C and Si/C-900 because of the presence of coated carbon using sucrose. Figure 2b presents the Raman spectra of bulk Si, Si/C, Si/C-900, Si/C + C-900, and Si-400. The two peaks at about 515.2 and 965.5 cm^{-1} for all samples are characteristic of Si.[9] The observation of a double maximum on a wide feature at 1350 cm^{-1} (known as the D band) and 1590 cm^{-1} (known as the G band) is characteristic of the presence of carbon materials in Si/C, Si/C-900, and Si/C + C-900 samples.[3g] For Si/C-900 and Si/C + C-900 obtained by carbonization at 900 °C, the peaks of the G band and D band become stronger and the ratio of their intensities (I_G/I_D) increase from 0.51 for Si/C to 0.66 for Si/C-900 and 0.68 for Si/C + C-900, implying a high degree of graphitic content of the carbon layer after high-temperature carbonization. After calcination at 400 °C in air, both D and G bands for Si-400 disappeared, indicating the removal of the carbon layers. TG curves of Si/C, Si/C-900, Si/C + C-900, and Si/C + C-900-HF (Supporting Information, Figure S3) shows that their carbon content is 18.5, 17.7, 36.8, and 35.9 wt %, respectively. The combustion temperature of carbon layers for Si/C is remarkably lower than that of the other samples, suggesting the lower graphitic degree of its carbon layer as observed with XRD and Raman analysis. Furthermore, there is no obvious weight loss for Si-400, suggesting the carbon of Si/C is completely removed at 400 °C in air. The surface area of the Si/C was 65.5 $m^2 g^{-1}$, which was decreased to 58.6 $m^2 g^{-1}$ for Si/C-900, to 18.4 $m^2 g^{-1}$ for Si/C + C-900, to 20.8 $m^2 g^{-1}$ for Si/C + C-900-HF, and to 13.9 $m^2 g^{-1}$ for Si-400, which is possibly due to the increase of carbon amount and density. The TEM image in Figure 2c shows that Si/C-900 has a porous structure with a pore size of about 2–5 μm. The similar porous structure also exists within Si/C, Si/C + C-900, Si/C + C-900-HF, and Si-400 (Supporting Information, Figure S4). Figure 2d shows the high-resolution TEM image of Si/C-900. The measured lattice plane distance is about 0.31 nm, which is in agreement with the (111) plane distance of Si and the Si is coated with amorphous carbon. The elemental mapping image also shows that Si/C-900 has a uniform elemental distribution of C and Si, and EDX spectroscopy indicates that this sample is composed of C, Si, and O at an approximate mass ratio of 25:73:2, in which, the Si and C elements are predominant (Supporting Information, Figure S5).

Figure 3a shows the first discharge and charge capacities of bulk Si, Si-400, Si/C, Si/C-900, Si/C + C-900, Si/C + C-900-HF, which are about 3372.5 and 1372.5, 3573.1 and 1877.4, 2646.1 and 1521.9, 2609.5 and 1453.8, 1385.1 and 949.4, and 1241.7 and 856.5 mA h g^{-1}, with an initial Coulombic efficiency of 40.7, 52.5, 57.5, 55.7, 68.5, and 69.0 %, respectively. The irreversible capacity can be attributed to the formation of solid electrolyte interphase (SEI) on the surface of an electrode, and also to the irreversible insertion of lithium ions into the Si particles.[3d] The improved initial Coulombic efficiency of Si/C, Si/C-900, Si/C + C-900, and Si/C + C-900-HF as compared to the bulk Si

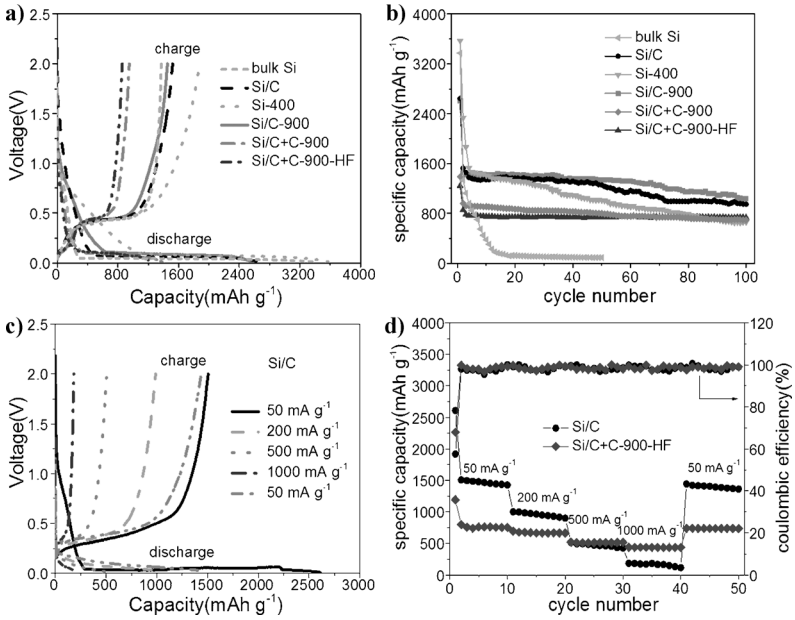

Figure 3. Electrochemical properties: a) the initial discharge–charge and b) cycling property of bulk Si, Si/C, Si/C-900, Si/C + C-900, Si/C + C-900-HF, and Si-400 at the current density of 50 mA g^{-1}, c) the discharge–charge curves of Si/C at different current densities, and d) the rate performance of Si/C and Si/C + C-900-HF.

 © 2014 Wiley-VCH Verlag GmbH & Co. KGaA, Weinheim

and Si-400 is associated with the carbon-coated layers, which reduce the occurrence of side reactions with the electrolyte.[3n] The discharge–charge curves show a lithiation (formation of Si-Li alloy by Li insertion) voltage plateau at about 0.05–0.08 V, and a delithiation (Li extraction) voltage plateau at about 0.43–0.50 V. The carbon delithiation voltage plateau observed at about 0.05–0. 2 V is too small to be visible for Si/C, Si/C-900, Si/C + C-900, and Si/C + C-900-HF, because of the very small contribution of carbon to the overall anode capacity.[3j] On the other hand, although it is believed that the contribution to the overall capacity of Si-based anodes mainly comes from Si, this Si contribution is different among above samples because they experienced different post treatment processes, which normally lead to the change in surface chemistry, porous structure, content, crystallinity, and conductivity. As shown in Figure 3b, after 100 cycles, the discharge capacity of Si/C, Si/C-900, Si/C + C-900, and Si/C + C-900-HF is 996.5, 1036.6, 694.2, and 732.1 mAh g^{-1}, respectively, which are much higher than those of Si-400 (657.5 mA h g^{-1} after 100 cycles) and bulk Si (90.2 mA h g^{-1} after 50 cycles). Meanwhile, an average capacity fading rate of Si/C, Si/C-900, Si/C + C-900, and Si/C + C-900-HF is around 0.35, 0.29, 0.27, and 0.15 %/cycle, respectively, which are much lower than those of Si-400 (0.55 %/cycle) and bulk Si (1.87 %/cycle). The improved cycling performance for Si/C-900 over Si/C is because of the higher graphitic degree of carbon layer in the former.[10a] Among these materials, Si/C + C-900-HF has the best cycling performance. The volumetric capacity of Si/C + C-900-HF after 100 cycles is calculated to be 627.5 mA h cm^{-3} (with respect to the total volume of the electrode including active materials, acetylene black, and PVDF), which is lower than that of the C-Si bottom-up-assembled nanocomposite spherical granules (initial charge capacity of 1270 mA h cm^{-3})[3j] and graphene encapsulated Si nanoparticles (initial charge capacity of 1016 mA h cm^{-3}),[3k] but higher than nano-Si coated with polymeric aluminum glycerol (569 mA h cm^{-3} after 150 cycles).[10b] Figure 3c reveals that the discharge capacity of Si/C is 2610.5, 999.2, 515.3, 185.1, and 1442.1 mA h g^{-1} and the charge capacity is 1505.6, 988.3, 506.1, 181.9, and 1437.4 mA h g^{-1} at the current densities of 50, 200, 500, 1000, and 50 mA g^{-1}, respectively. The charge capacity at 200, 500, and 1000 mA g^{-1} is about 65.6, 33.6, and 12.1 % of that at 50 mA g^{-1}, respectively. This good rate capability is attributed to the interconnected porous structure and the coated carbon layer that provide fast lithium ion mobility. As a result, Li ions can rapidly reach the active anode material.[1l,3n] Figure 3d shows that, after 10 cycles at 50, 200, 500, 1000, and 50 mA g^{-1}, Si/C delivers a discharge capacity of 1425.2, 899.1, 429.7, 116.7, and 1361.0 mA h g^{-1}, while that of Si/C + C-900-HF is 748.4, 651.5, 516.1, 437.2, and 732.1 mA h g^{-1}, respectively, suggesting a better rate performance of Si/C + C-900-HF at different current densities. This may be attributed to the higher carbon content and graphitic degree as well as the increased interfacial space formed between Si and carbon layer in Si/C + C-900-HF.[6] This structure can absorb the huge volume change of Si during Li insertion and extraction reactions, and hinder the cracking or crumbling of the electrode, thus promoting the cycling stability. Furthermore, the higher carbon content can improve the conductivity to enhance the rate performance. However, it should be mentioned that the discharge capacities of these Si/C anode materials are still lower than those of the porous Si nanowires[10c] and three-dimensional porous carbon-coated Si particles,[3n] probably because of the use of different binders,[10c] electrolytes,[3n] and loadings of active materials,[3n] as well as the difference in Si morphology and testing techniques.[10c] After first discharge and charge, the cross-sectional SEM images of electrode disks containing Si/C-900 (Supporting Information, Figure S6a1–c1), Si/C + C-900 (Figure S6a2–c2), and Si/C + C-900-HF (Figure S6a3–c3) shows that the increase of their thickness is totally less than 50 % and particularly the thickness of Si/C + C-900-HF electrode disk almost has no visible change, even after 100 charge–discharge cycles (Figure S6d3). Moreover, after 100 charge–discharge cycles, SEM images of charged Si/C (Figure S7a), Si/C-900 (Figure S7b), Si/C + C-900 (Figure S7c), and Si/C + C-900-HF (Figure S7d) scraped from the disks show that the original textural properties of these materials such as the particle size and shape, and the structural integrity are still well-retained, indicating the good structural stability of these materials. Furthermore, the volume expansion/contraction of these Si-based materials after charge or discharge cycles should be carefully investigated and correlated with their cyclic difference.

Although the obtained samples show a much larger capacity than that of the commercial graphite anodes (372 mA h g^{-1}), their relatively low initial coulombic efficiency should be improved further prior to the practical use. However, unlike other reported preparation processes of nanostructured porous Si/C anodes such as CVD,[3j] Mg metal reduction,[4a,b] and the wet-chemical etching method with noble metals such as Ag and Au,[3l] our synthesis approach may be readily scaled up with comparable cost and scalability to the commercial graphite anodes when using abundant metallurgical-grade Si, diverse Cu-based catalysts, mild reaction conditions, and industrial reactor bed in organosilane industry.

In summary, we have developed a novel scalable route to prepare porous Si/C anode materials by the Rochow reaction under the mild reaction conditions (325–450 °C, atmospheric pressure, and various Cu-based catalysts). These obtained Si/C materials are composed of interconnected porous Si and conductive carbon-coated layer. After simple post treatment, they exhibit good electrochemical performance with a high reversible capacity, long cycle life, and rate performance, making them promising for the next generation Li ion batteries. More importantly, the large scale preparation of nanostructured porous Si materials used in other areas, such as nanoelectronics, photonics, sensors, delivery systems, and solar cells, is also possible if the Cu-based catalyst particles are well patterned on the specific Si substrates.

Received: December 1, 2013
Revised: February 21, 2014
Published online: April 2, 2014

Keywords: anode materials · heterogeneous catalysis · lithium storage · porous nanostructures · silicon

© 2014 Wiley-VCH Verlag GmbH & Co. KGaA, Weinheim

[1] a) Y. Cui, C. M. Lieber, *Science* **2001**, *291*, 851; b) A. Blanco, E. Chomski, S. Grabtchak, M. Ibisate, S. John, S. W. Leonard, C. Lopez, F. Meseguer, H. Miguez, J. P. Mondia, G. A. Ozin, O. Toader, H. M. Van Driel, *Nature* **2000**, *405*, 437; c) V. S. Y. Lin, K. Motesharei, K. P. S. Dancil, M. J. Sailor, M. R. Ghadiri, *Science* **1997**, *278*, 840; d) A. M. Ruminski, B. H. King, J. Salonen, J. L. Snyder, M. J. Sailor, *Adv. Funct. Mater.* **2010**, *20*, 2874; e) B. Z. Tian, T. Cohen-Karni, Q. Qing, X. J. Duan, P. Xie, C. M. Lieber, *Science* **2010**, *329*, 830; f) B. Z. Tian, X. L. Zheng, T. J. Kempa, Y. Fang, N. F. Yu, G. H. Yu, J. L. Huang, C. M. Lieber, *Nature* **2007**, *449*, 885; g) A. I. Hochbaum, R. K. Chen, R. D. Delgado, W. J. Liang, E. C. Garnett, M. Najarian, A. Majumdar, P. D. Yang, *Nature* **2008**, *451*, 163; h) J. H. Park, L. Gu, G. von Maltzahn, E. Ruoslahti, S. N. Bhatia, M. J. Sailor, *Nat. Mater.* **2009**, *8*, 331; i) M. McDowell, S. Lee, W. Nix, Y. Cui, *Adv. Mater.* **2013**, *25*, 4966; j) I. Kovalenko, B. Zdyrko, A. Magasinski, B. Hertzberg, Z. Milicev, R. Burtovyy, I. Luzinov, G. Yushin, *Science* **2011**, *334*, 75; k) C. M. Park, J. H. Kim, H. Kim, H. J. Sohn, *Chem. Soc. Rev.* **2010**, *39*, 3115; l) J. Cho, *J. Mater. Chem.* **2010**, *20*, 4009.

[2] a) M. Armand, J. M. Tarascon, *Nature* **2008**, *451*, 652; b) H. Wu, Y. Cui, *Nano Today* **2012**, *7*, 414; c) S. W. Lee, M. T. McDowell, L. A. Berla, W. D. Nix, Y. Cui, *Proc. Natl. Acad. Sci. USA* **2012**, *109*, 4080.

[3] a) Y. Park, N. S. Choi, S. Park, S. H. Woo, S. Sim, B. Y. Jang, S. M. Oh, S. Park, J. Cho, K. T. Lee, *Adv. Energy Mater.* **2013**, *3*, 206; b) C. K. Chan, H. L. Peng, G. Liu, K. McIlwrath, X. F. Zhang, R. A. Huggins, Y. Cui, *Nat. Nanotechnol.* **2008**, *3*, 31; c) H. Ma, F. Y. Cheng, J. Chen, J. Z. Zhao, C. S. Li, Z. L. Tao, J. Liang, *Adv. Mater.* **2007**, *19*, 4067; d) H. Wu, G. Chan, J. W. Choi, I. Ryu, Y. Yao, M. T. McDowell, S. W. Lee, A. Jackson, Y. Yang, L. B. Hu, Y. Cui, *Nat. Nanotechnol.* **2012**, *7*, 309; e) H. Kim, M. Seo, M. H. Park, J. Cho, *Angew. Chem.* **2010**, *122*, 2192; *Angew. Chem. Int. Ed.* **2010**, *49*, 2146; f) A. Esmanski, G. A. Ozin, *Adv. Funct. Mater.* **2009**, *19*, 1999; g) Z. Zhang, M. Zhang, Y. Wang, Q. Tan, X. Lv, Z. Zhong, H. Li, F. Su, *Nanoscale* **2013**, *5*, 5384; h) X. Zhu, H. Chen, Y. Wang, L. Xia, Q. Tan, H. Li, Z. Zhong, F. Su, X. Zhao, *J. Mater. Chem. A* **2013**, *1*, 4483; i) D. S. Jung, T. H. Hwang, S. B. Park, J. W. Choi, *Nano Lett.* **2013**, *13*, 2092; j) A. Magasinski, P. Dixon, B. Hertzberg, A. Kvit, J. Ayala, G. Yushin, *Nat. Mater.* **2010**, *9*, 353; k) J. Ji, H. Ji, L. Zhang, X. Zhao, X. Bai, X. Fan, F. Zhang, R. S. Ruoff, *Adv. Mater.* **2013**, *25*, 4673; l) D. Y. Chen, X. Mei, G. Ji, M. H. Lu, J. P. Xie, J. M. Lu, J. Y. Lee, *Angew. Chem.* **2012**, *124*, 2459; *Angew. Chem. Int. Ed.* **2012**, *51*, 2409; m) H. Wu, G. Yu, L. Pan, N. Liu, M. McDowell, Z. Bao, Y. Cui, *Nat. Commun.* **2013**, *4*, 1943; n) H. Kim, B. Han, J. Choo, J. Cho, *Angew. Chem.* **2008**, *120*, 10305; *Angew. Chem. Int. Ed.* **2008**, *47*, 10151.

[4] a) N. A. Liu, K. F. Huo, M. T. McDowell, J. Zhao, Y. Cui, *Sci. Rep.* **2013**, *3*, 1919; b) D. S. Jung, M. H. Ryou, Y. J. Sung, S. B. Park, J. W. Choi, *Proc. Natl. Acad. Sci. USA* **2013**, *110*, 12229; c) W. S. Chang, C. M. Park, J. H. Kim, Y. U. Kim, G. Jeong, H. J. Sohn, *Energy Environ. Sci.* **2012**, *5*, 6895; d) M. Gauthier, D. Mazouzi, D. Reyter, B. Lestriez, P. Moreau, D. Guyomard, L. Roue, *Energy Environ. Sci.* **2013**, *6*, 2145.

[5] a) E. G. Rochow, *J. Am. Chem. Soc.* **1945**, *67*, 963; b) J. Yu, H. Zhan, Y. Wang, Z. Zhang, H. Chen, H. Li, Z. Zhong, F. Su, *J. Power Sources* **2013**, *228*, 112.

[6] B. Wang, X. Li, X. Zhang, B. Luo, Y. Zhang, L. Zhi, *Adv. Mater.* **2013**, *25*, 3560.

[7] a) Z. Zhang, H. Che, Y. Wang, J. Gao, L. Zhao, X. She, J. Sun, P. Gunawan, Z. Zhong, F. Su, *Ind. Eng. Chem. Res.* **2012**, *51*, 1264; b) Z. Zhang, H. Che, Y. Wang, J. Gao, X. She, J. Sun, Z. Zhong, F. Su, *RSC Adv.* **2012**, *2*, 2254; c) W. Liu, L. Jia, Y. Wang, L. Song, Y. Zhu, X. Chen, Z. Zhong, F. Su, *Ind. Eng. Chem. Res.* **2013**, *52*, 6662; d) X. Chen, L. Jia, Y. Wang, L. Song, Y. Zhu, W. Liu, Z. Zhong, F. Su, *J. Colloid Interface Sci.* **2013**, *404*, 16.

[8] a) W. F. Banholzer, N. Lewis, W. Ward, *J. Catal.* **1986**, *101*, 405; b) T. C. Frank, K. B. Kester, J. L. Falconer, *J. Catal.* **1985**, *91*, 44; c) Z. Zhang, H. Che, J. Gao, Y. Wang, X. She, J. Sun, P. Gunawan, Z. Zhong, F. Su, *Catal. Sci. Technol.* **2012**, *2*, 1207.

[9] R. M. S. dos Reis, R. L. Maltez, E. C. Moreira, Y. P. Dias, H. Boudinov, *Appl. Surf. Sci.* **2012**, *258*, 7395.

[10] a) R. Yi, F. Dai, M. Gordin, H. Sohn, D. Wang, *Adv. Energy Mater.* **2013**, *3*, 1507; b) D. Piper, J. Travis, M. Young, S. Son, S. Kim, K. Oh, S. George, C. Ban, S. Lee, *Adv. Mater.* **2013**, *26*, 1596; c) M. Y. Ge, J. P. Rong, X. Fang, C. W. Zhou, *Nano Lett.* **2012**, *12*, 2318.

 © 2014 Wiley-VCH Verlag GmbH & Co. KGaA, Weinheim